

PAPER: CLASSICAL STATISTICAL MECHANICS, EQUILIBRIUM AND NON-EQUILIBRIUM

Effect of interactions for one-dimensional asymmetric exclusion processes under periodic and bath-adapted coupling environment

To cite this article: Tripti Midha *et al* *J. Stat. Mech.* (2018) 043205

View the [article online](#) for updates and enhancements.

Related content

- [Theoretical investigations of asymmetric simple exclusion processes for interacting oligomers](#)
Tripti Midha, Luiza V F Gomes, Anatoly B Kolomeisky *et al.*
- [The effect of side motion in the dynamics of interacting molecular motors](#)
Tripti Midha, Arvind Kumar Gupta and Anatoly B Kolomeisky
- [Correlations and symmetry of interactions influence collective dynamics of molecular motors](#)
Daniel Celis-Garza, Hamid Teimouri and Anatoly B Kolomeisky

Recent citations

- [Theoretical investigations of asymmetric simple exclusion processes for interacting oligomers](#)
Tripti Midha *et al*



IOP | ebooks™

Bringing you innovative digital publishing with leading voices to create your essential collection of books in STEM research.

Start exploring the collection - download the first chapter of every title for free.

PAPER: Classical statistical mechanics, equilibrium and non-equilibrium

Effect of interactions for one-dimensional asymmetric exclusion processes under periodic and bath-adapted coupling environment

Tripti Midha¹, Anatoly B Kolomeisky² and Arvind Kumar Gupta¹

¹ Department of Mathematics, Indian Institute of Technology Ropar, Rupnagar-140001, Punjab, India

² Department of Chemistry and Center for Theoretical Biological Physics, Rice University, Houston, Tx 77005, United States of America

E-mail: akgupta@iitrpr.ac.in

Received 14 November 2017

Accepted for publication 7 February 2018

Published 10 April 2018

Online at stacks.iop.org/JSTAT/2018/043205

<https://doi.org/10.1088/1742-5468/aab022>



CrossMark

Abstract. Stimulated by the effect of the nearest neighbor interactions in vehicular traffic and motor proteins, we study a 1D driven lattice gas model, in which the nearest neighbor particle interactions are taken in accordance with the thermodynamic concepts. The non-equilibrium steady-state properties of the system are analyzed under both open and periodic boundary conditions using a combination of cluster mean-field analysis and Monte Carlo simulations. Interestingly, the fundamental diagram of current versus density shows a complex behavior with a unimodal dependence for attractions and weak repulsions that turns into the bimodal behavior for stronger repulsive interactions. Specific details of system-reservoir coupling for the open system have a strong effect on the stationary phases. We produce the steady-state phase diagrams for the bulk-adapted coupling to the reservoir using the minimum and maximum current principles. The strength and nature of interaction energy has a striking influence on the number of stationary phases. We observe that interactions lead to correlations having a strong impact on the system dynamical properties. The correlation between any two sites decays exponentially as the distance between the sites increases. Moreover, they are found to be *short-range* for repulsions and *long-range* for attractions. Our results also suggest that repulsions and

Effect of interactions for one-dimensional asymmetric exclusion processes under periodic attractions asymmetrically modify the dynamics of interacting particles in exclusion processes.

Keywords: correlation functions, exclusion processes, molecular motors, traffic models

Contents

| | |
|--|-----------|
| 1. Introduction | 2 |
| 2. Theoretical description | 4 |
| 2.1. Model..... | 4 |
| 3. Bulk current-density relation: mean-field analysis | 5 |
| 3.1. Two-cluster mean-field theory | 7 |
| 3.2. Three cluster mean-field theory | 11 |
| 4. Particles locomotion in open system | 13 |
| 5. Bulk-adapted coupling and NESS phases | 14 |
| 6. Correlations | 16 |
| 7. Conclusion | 18 |
| Acknowledgment | 19 |
| Appendix. Calculation of t_n | 19 |
| References | 20 |

1. Introduction

Driven diffusive systems are of fundamental importance for the extensive study of non-equilibrium statistical properties. They embrace the non-equilibrium steady state (NESS) behavior of various transport processes in Physics, Chemistry and Biology such as motion of molecular motors along filaments [1], mRNA translation [2, 3], gel electrophoresis [4], vehicular traffic [5], pedestrian flow [6], etc. These processes can be well studied and interpreted by low-dimensional models involving biased hopping of particles under a driven electric field [7]. Such environment of particle hopping embarks the non-zero constant steady-state current through the system, which is a signature of non-equilibrium systems. Totally asymmetric simple exclusion process (TASEP), the minimal model in the class of driven lattice gas models, has extensively provided various interesting nontrivial facts of non-equilibrium systems and transport mechanisms [8].

TASEP, first introduced in 1968 to model protein synthesis by ribosomes [9], enjoys the paradigmatic status for exploring NESS properties of transport systems. Basically, the simple TASEP describes the unidirectional particle hopping on a one-dimensional (1D) lattice under the hard-core exclusion principle. The type of boundary condition

to the lattice plays an important role in determining the steady-state properties. For periodic boundary conditions, where the total number of particles are conserved in the system, all particle configurations are equally likely [10]. In open systems, the two ends of the lattice are coupled to reservoirs of fixed density and the distribution of the microstates is non-uniform. Such open boundary conditions are responsible for various interesting features such as boundary induced phase transitions [11, 12], shock dynamics [13], shock and pattern formation [14], which are not observed in closed TASEP. The simple TASEP has been well explored in the literature using several exact as well as approximate analytical methods such as matrix product ansatz [15], domain wall theory [16], recursion methods [17] and mean-field theory [17]. For reviews on TASEP, one can refer [10, 18, 19].

Many realistic processes such as traffic flow, collective dynamics of molecular motors along filaments, etc, function under the presence of repulsive and attractive interaction energy between the nearest neighboring particles [20–27]. For considering the effect of inter-particle interactions, the TASEP in which particles interact only with hard-core repulsions, needs to be modified. In this direction, several studies and variants of TASEP for periodic as well as open boundary conditions have been reported in the literature [13, 28–33, 35]. For open systems, where the bulk hopping rates depend on the configuration of four consecutive lattice sites [13, 28, 29, 31–33], an interesting feature of a double-hump like structure appeared in the fundamental diagram of current versus density. In these systems, the description of NESS properties, the phase diagrams of the bulk density, in particular, was made using maximum and minimum current principles [11, 28]. Particularly, in [31–33], the application of the extremal current principles demanded a very specific set up of reservoir coupling, called the bulk-adapted coupling, in which the criterion of ejection and injection rates close to the system boundaries is similar to the bulk dynamics. Moreover, the hopping rules in [31–33] satisfied certain constraints [33, 34] and the systems were analyzed only for repulsive interactions using the time-dependent density functional approach that approximate the non-equilibrium distribution by the Boltzmann probability with an effective time-dependent external potential. As the experiments on motor protein suggest a possibility of attractive interaction among them, it becomes necessary to examine the role of attractions in the collective motion of molecular motors [25–27]. Furthermore, many other existing theoretical studies on interactive exclusions systems are completely phenomenological [13, 28, 29, 35]. It is known that the inter-molecular interactions influence various chemical transitions such as chemical transformations during hydrolysis, association and dissociation from the tracks, etc, occurring among the motor proteins at the microscopic level. So, it is important to regard the quantitative description of such chemical processes in the investigation of collective dynamics of interacting particles [24].

More recently, a variant of open TASEP considering the particle-particle repulsive as well as attractive interactions in a thermodynamic consistent fashion has been introduced [36, 37]. Here, creating and breaking of bonds between nearest neighbors are viewed as opposite chemical reactions, which allow one to apply the detailed balance-like arguments. In [36], the model was analyzed using a cluster mean-field approach that considers some correlations. However, the approach had some limitations. Firstly, it did not explicitly calculate the bulk current-density relationship. Secondly, it failed to capture the effect of interaction energy on the density corresponding to the maximal

current. As a result, the bulk particle current had a single maximum at $\rho = 0.5$ irrespective of any interaction strength. Later, in [37], a new approach called modified cluster mean-field was introduced. The approach could account for some correlations and found a single point of maximum for particle current, which varied with respect to the interaction energy. Also, the phase diagram in [36, 37] had three generic phases, which is unlike the earlier models considering the effect of interactions [13, 28, 29, 31–33]. In addition, the [36, 37] considered only the open boundary conditions and did not analyze the bulk current-density relation. The theoretical approaches were also approximate, which had only a qualitative agreement with simulations. This motivates us to analyze the collective dynamics of interacting particles for periodic as well as open boundary conditions with a stronger approximate theory than in [36, 37].

In this paper, we first discuss the TASEP model, where particle-particle interactions are taken in accordance with the thermodynamic consistent rules in section 2. We, then, analyze the bulk current-density relation in section 3 with much stronger cluster mean-field theories. We also validate our results with extensive Monte Carlo simulations. The NESS properties of the open system with the bulk-adapted coupling to the reservoirs are discussed in sections 4 and 5. Further, the correlation between two sites separated by an arbitrary distance is calculated and analyzed in section 6. Finally, we conclude in section 7.

2. Theoretical description

2.1. Model

We consider driven particle unidirectional transport process on a 1D lattice chain with N sites, each site being occupied by at most one particle under the exclusion principle. The microstate of the system is characterized by the set of occupation number $\tau = \{\tau_i\}$ ($i = 1, 2, \dots, N$), each of which is either zero (vacant site) or one (occupied site). In the process, particles hop in a random-sequential manner to their next site with rates depending on the occupancy state of the nearest and next-nearest-neighbor site. It is presumed that an interaction energy E is associated with the bond connecting two nearest neighboring particles, where $E > 0$ ($E < 0$) corresponds to attractions (repulsions) [36]. In such scenario, the dynamical rules of the model are defined as follows. If the particle hopping leads to the bond formation (destruction), the hopping rate is q (r). Otherwise, when bond formation and destruction occur simultaneously or neither of them occurs, the hopping rate is 1. The four possible hopping rates of a particle at an i th site to the vacant $(i + 1)$ th site depending on the occupancy state of $(i - 1)$ th and $(i + 2)$ th sites are shown in figure 1. The phenomenon of creating and breaking of bonds between pair of particles is viewed as reversible chemical reaction and thus the rates q and r follow the relation $\frac{q}{r} = e^E$ [36], where E is expressed in units of $k_B T$. The explicit values of q and r , which are $q = e^{\theta E}$ and $r = e^{(\theta-1)E}$, are obtained by introducing a dimensionless splitting parameter θ ($0 \leq \theta \leq 1$). This parameter quantifies how much the transitions rates are affected by the interactions. The above choice of hopping rules preserves the particle-hole symmetry in the system. In the absence of energy (i.e. $q = r = 1$), the bulk dynamics of our model reduces to the simple TASEP [10]. It is




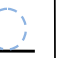



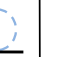
























| t | | | | W | $t + 1$ | | | |
|---|---|---|---|-----|---|--|---|---|
| $(i - 1)$ | i | $(i + 1)$ | $(i + 2)$ | | $(i - 1)$ | i | $(i + 1)$ | $(i + 2)$ |
|  |  |  |  | 1 |  |  |  |  |
|  |  |  |  | q |  |  |  |  |
|  |  |  |  | r |  |  |  |  |
|  |  |  |  | 1 |  |  |  |  |

Figure 1. Sketch of evolution of four different clusters with i th site occupied (filled circle) and $(i + 1)$ th site empty (dotted circle) from the t th time step to the $(t + 1)$ th time step with the corresponding transition rates denoted by W .

important to note that theoretical models considered in [31–33] correspond to the case $\theta = 0.5$ in our language. But these papers also considered only the repulsive interactions, while our model is analyzed for both attractive and repulsive interactions.

The proposed model suits well to analyze the collective dynamics of interacting molecular motors [36, 37]. Moreover, the model also interprets the vehicular traffic flow in the case of repulsive interactions. A driver generally slows down his vehicle, if a slowly moving vehicle is found some distance ahead, implying $q < 1$ or he speeds up in the case of a rear vehicle honking its horn, yielding $r > 1$ [29]. However, when either both the above cases occur simultaneously or neither of them occurs, a vehicle can neither speed up nor slow down, thus moves with its usual rate 1. Similar bulk dynamics has been considered in [36, 37]. However, our model differs from these references in the context of the boundary conditions and the cluster mean-field approach, which together contributes to interesting new findings. We have employed the periodic boundary conditions and measured the effect of interactions on the system bulk properties by analyzing the current-density relation, commonly known as the fundamental diagram in the context of vehicular traffic. Also, the *bulk-adapted coupling* to the reservoirs is undertaken to study the interplay of particles' interactions among themselves and with the reservoirs of fixed particle densities.

3. Bulk current-density relation: mean-field analysis

In this section, we calculate and analyze the bulk current-density relation in the NESS using various mean-field analysis. We denote the steady-state probability of a cluster, $(\tau_i, \tau_{i+1}, \dots, \tau_{i+n-1})$, of length n (n -cluster) by $P(\tau_i, \tau_{i+1}, \dots, \tau_{i+n-1})$. According to the system dynamics, the bulk particle current in terms of probabilities can be written as

$$J = P(0, 1, 0, 0) + qP(0, 1, 0, 1) + rP(1, 1, 0, 0) + P(1, 1, 0, 1). \quad (1)$$

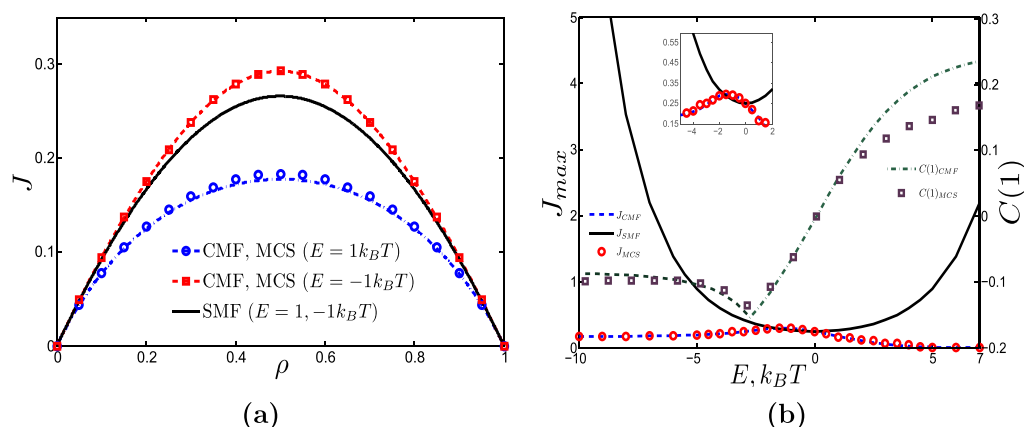


Figure 2. (a) Mean-field analysis and simulation results of the fundamental diagram of stationary particle current (J) versus particle density (ρ) for a fixed $\theta = 0.5$. (b) On the left : particle maximal current (J_{\max}) as a function of interaction energy (E) and on the right: correlation curve as a function of interaction energy (E). Dotted and solid lines, respectively, denote the results of cluster mean-field and simple mean-field theories, whereas symbols represent the simulation results.

The computation of the current requires the determination of the probability of 4-clusters or the four point spatial correlators $\langle \tau_{i-1} \tau_i \tau_{i+1} \tau_{i+2} \rangle$. We first review the particle current using simple mean-field (SMF) theory in which the probability of an n -cluster is splitted into the product of the probability of every single site of the cluster i.e. $P(\tau_i, \tau_{i+1}, \dots, \tau_{i+n-1}) \approx P(\tau_i) P(\tau_{i+1}) \dots P(\tau_{i+n-1})$. Since the particle density at every site is associated with its average occupancy i.e. $\rho = \langle \tau \rangle$, where ρ is the system density, we have $P(1) = \rho$ and $P(0) = 1 - \rho$. This yields the following relation between the bulk particle current and the density:

$$J(\rho) = [\rho(1 - \rho)((1 - \rho)^2 + \rho^2)] + (q + r)\rho^2(1 - \rho)^2. \quad (2)$$

Clearly, the particle-hole symmetry in the bulk dynamics is preserved as $J(\rho) = J(1 - \rho)$. We plot the above density-current relation for a repulsive as well as attractive interaction energy with a fixed $\theta = 0.5$, which incorporates the maximum and equal effect of energy E on the rates q and r , and compare the results with Monte Carlo simulations as shown in figure 2(a). Clearly, for both repulsions and attractions, the SMF results fail to match with the simulations. Further, it can be seen that the maximal particle current, $J_{\max} = \frac{1}{8} + \frac{(q+r)}{16}$ obtained for $\rho = 0.5$ in equation (2), becomes unbounded for $|E| \gg 1$. This is physically impossible, as for large attractions, the particles group together to form clusters, which hinders their movement and for stronger repulsions, the situation reduces to TASEP with dimers, where the particle current is finite (see figure 2(b)) [36, 41]. The reason for the inadequacy of the SMF approach in determining the particle current is its ignorance of the correlations between two neighboring sites.

For a reasonable analysis of current-density relation, we apply cluster mean-field theory that considers some correlations between neighboring sites. In general, in the n -cluster mean-field theory, the master equation governing the time evolution of any n -cluster probability, $P(\tau, t)$ is given as

$$\frac{\partial P(\tau, t)}{\partial t} = \underbrace{\sum_{\tau' \neq \tau} W(\tau' \rightarrow \tau) P(\tau', t)}_{\text{Gain term}} - \underbrace{\sum_{\tau' \neq \tau} W(\tau \rightarrow \tau') P(\tau, t)}_{\text{Loss term}}, \quad (3)$$

where τ' is some $(n+k)$ -cluster ($k \geq 1$) giving rise to or arising from the n -cluster, τ , and $W(\tau' \rightarrow \tau)$ represents the transition rate from cluster τ' to cluster τ . In the steady state, the probability $P(\tau')$ of a $(n+k)$ cluster, given as $\tau' = (\tau_1, \tau_2, \dots, \tau_{n+k})$, is split into the product of the probability of n -clusters such that each pair of adjacent n -clusters have $(n-1)$ common sites [38]. Firstly, we consider the case of $n=2$ and employ the two-cluster mean-field (two-cmf) theory to obtain the bulk current-density relation.

3.1. Two-cluster mean-field theory

Under the two-cluster mean-field approximation, the joint probability of any 4-cluster $(\tau_{i-1}, \tau_i, \tau_{i+1}, \tau_{i+2})$ is mathematically expressed as

$$P(\tau_{i-1}, \tau_i, \tau_{i+1}, \tau_{i+2}) = P(\tau_{i-1} | \underline{\tau_i}) P(\tau_i | \underline{\tau_{i+1}}) P(\tau_{i+1}, \tau_{i+2}), \quad (4)$$

where

$$P(\tau_{i-1} | \underline{\tau_i}) = \frac{P(\tau_{i-1}, \tau_i)}{\sum_{\tau_{i-1} \in \{0,1\}} P(\tau_{i-1}, \tau_i)} \quad (5)$$

is the conditional two-cluster probability. For simplicity, we denote the possible distinct two-cluster probabilities $P(1, 1)$, $P(1, 0)$ and $P(0, 0)$ by x , y and z , respectively. Clearly, $P(1, 0) = P(0, 1)$ due to the particle-hole symmetry in the system. The definition of density and the Kolmogorov consistency conditions [39] give the following two equations about x , y and z :

$$x + y = \rho, \quad (6)$$

$$y + z = 1 - \rho. \quad (7)$$

Using equations (4)–(7) in equation (1), the bulk particle current reduces to

$$J = \frac{y^2 z + qy^3 + rxyz + xy^2}{\rho(1 - \rho)}. \quad (8)$$

To obtain the bulk current-density relation, we require x , y and z explicitly in terms of density ρ . For this, we compute the steady-state master equation for y using equation (3) as

$$rP(1, 1, 0, 0) - qP(0, 1, 0, 1) = 0.$$

Applying the two-cmf analysis (equations (4) and (5)) to the above equation yields

$$y^2 = \frac{rxz}{q}. \quad (9)$$

Equation (9) along with the equations (6) and (7) gives the following values of x , y and z in terms of ρ :

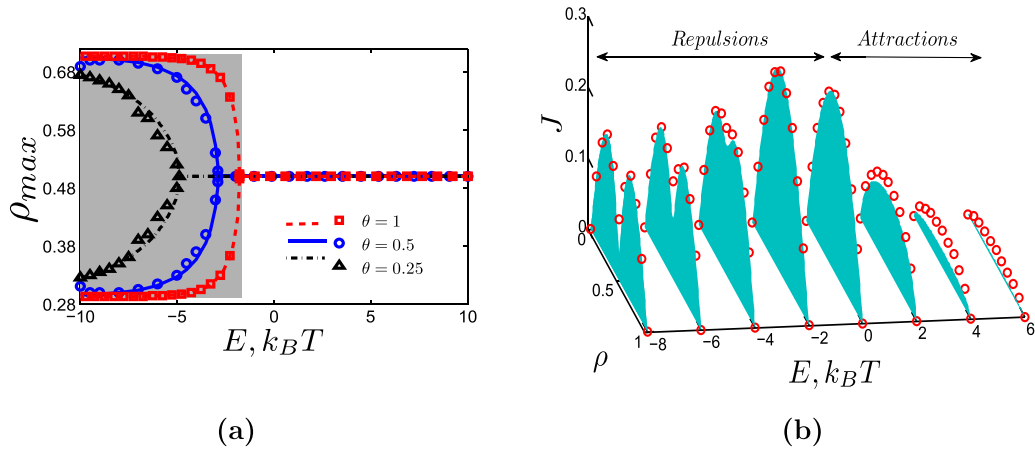


Figure 3. (a) Cluster mean-field analysis and simulations results of the particle density corresponding to maximal particle current with respect to interaction energy $E, k_B T$. (b) Particle current (J) as a function of interaction energy (E) and particle density (ρ); Symbols represent the simulation results.

$$x = \begin{cases} \frac{1}{2} \left(2\rho + \frac{r - \sqrt{r(r+4(q-r)\rho(1-\rho))}}{(q-r)} \right); & \text{if } q, r \neq 1 \\ \rho^2; & \text{if } q = r = 1, \end{cases} \quad (10)$$

$$y = \begin{cases} \frac{-r + \sqrt{r(r+4(q-r)\rho(1-\rho))}}{2(q-r)}; & \text{if } q, r \neq 1 \\ \rho(1 - \rho); & \text{if } q = r = 1, \end{cases} \quad (11)$$

$$z = \begin{cases} \frac{1}{2} \left(2(1 - \rho) + \frac{r - \sqrt{r(r+4(q-r)\rho(1-\rho))}}{(q-r)} \right); & \text{if } q, r \neq 1 \\ (1 - \rho)^2; & \text{if } q = r = 1. \end{cases} \quad (12)$$

Note that under the defined thermodynamically consistent relation, the rates q and r are not equal for any non-zero interaction energy, which justifies the above three equations. Substituting x, y and z in J , we get the following current-density relation:

$$J = \left(\frac{(\sqrt{r^2 + 4r\rho(q-r)(1-\rho)} - r)}{4(q-r)^3\rho(\rho-1)} \right) [4r\rho(q-1)(q-r)(\rho-1) + (\sqrt{r^2 + 4r\rho(q-r)(1-\rho)} - r)(2rq - q - r)]. \quad (13)$$

The above equation holds for any general value of interaction energy E and splitting parameter θ . It is worth to note that under the two-cluster mean-field theory, the maximal particle current does not increase without bound for $|E| \gg 1$ as shown in figure 2(b) and the results are also in agreement with the Monte Carlo simulations. Thus, the two-cmf theory overcomes the major drawback of SMF theory. We now

analyze the particle current by defining a new variable $X = \rho(1 - \rho)$, which on substituting in the equation (13) yields

$$J = \frac{r - \sqrt{r^2 + 4r(q-r)X}}{4(q-r)^3X} [4r(1-q)(q-r)X + (\sqrt{r^2 + 4r(q-r)X} - r) \times (2qr - q - r)]. \quad (14)$$

To obtain the extremal points in the current-density relation, we need to determine

$$\frac{\partial J}{\partial \rho} = \frac{\partial J}{\partial X} \frac{\partial X}{\partial \rho} = \frac{\partial J}{\partial X} (1 - 2\rho) = 0. \quad (15)$$

Clearly, $\rho = 0.5$ is always a critical point of the current-density relation. To obtain the other critical roots, we set $\frac{\partial J}{\partial X} = 0$ that yields the following quadratic equation in X :

$$(r + \sqrt{r^2 + 4r(q-r)X})^2 = \frac{2r(q+r-2qr)}{1-q}. \quad (16)$$

The two real roots of the above equation exist only for the interaction energy $E \leq E_c(\theta)$, where $E_c(\theta)$ is a critical interaction energy for $0 < \theta \leq 1$. Below and at $E_c(\theta)$, the bulk current-density relation has three extrema, while above $E_c(\theta)$, the number of extreme points of the bulk current-density relation reduces to one i.e. $\rho = 0.5$. We substitute $X = 0.25$, corresponding to the critical root $\rho = 0.5$, in equation (16), that leads to the following condition on the critical interaction energy:

$$(1-q) \left(1 + \sqrt{\frac{q}{r}}\right)^2 = 2 \left(\frac{q}{r} + 1 - 2q\right). \quad (17)$$

The above equation can be solved to determine the critical interaction energy, $E_c(\theta)$ for different values of θ . For example, for $\theta = 0.5$, the above equation gives $E_c = 2 \ln(\sqrt{5} - 2) \approx -2.885k_B T$, and this results has been already observed earlier in [31]. Similarly, for $\theta = 1$, it gives $E_c = 2 \ln(\sqrt{2} - 2) \approx -1.76k_B T$, while for $\theta = 0.25$, it gives $E_c \approx -4.87k_B T$ (see figure 3(a)). It is interesting to note that for $\theta = 0$ there will be no splitting of the unimodal curve into bimodal curve at any strength of the interaction. Further, the two critical densities of the current-density relation for the case of $E < E_c(\theta)$ are given as

$$\rho_{1,2}^* = \frac{1}{2} \left(1 \mp \sqrt{\frac{q(1-q^2) + 3r(1-q) - 5qr(1-q) - 2\sqrt{2r(1-q)^3(q+r-2qr)}}{(1-q)^2(r-q)}}\right). \quad (18)$$

These densities act as points of local maximum for $E \leq E_c(\theta)$, whereas for $E > E_c(\theta)$, the root $\rho_3 = 0.5$ becomes the point of maximum. Figure 3(a) shows the densities corresponding to the maximal current, denoted as ρ_{\max} , for various values of interaction energy E and splitting parameter θ . Both the analytic and simulation results in figure 3(a) indicate that for $E > E_c(\theta)$, ρ_{\max} acts as a single-valued function of E taking the constant value $\rho = 0.5$, while for $E \leq E_c(\theta)$, ρ_{\max} altered to multi-valued function, with two points of maximal current given by $\rho_{1,2}^*$. This is an interesting feature of the interacting particle system, which has not been observed earlier in [36, 37]. The thermodynamically consistent open boundary conditions and theoretical approaches

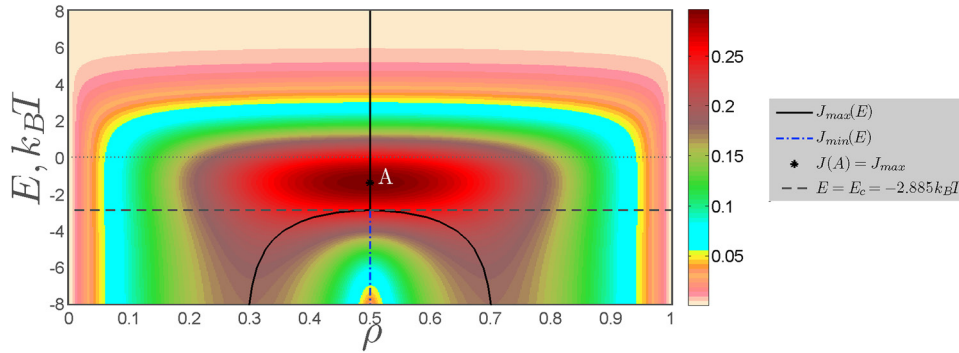


Figure 4. Density plot of particle current in the interaction energy (E) and particle density (ρ) phase plane.

such as cluster mean-field and modified cluster mean-field employed in these references produced a single maximum for particle current for any value of interaction energy. Whereas the above discussed two-cluster mean-field theory for the periodic interactive system yields two different densities, one being less than 0.5 and other being greater than 0.5, corresponding to maximal particle current in the case of sufficiently large repulsive interactions. The reason for such observation can be understood as follows. In the case of strong repulsions, the proposed model converges to TASEP with dimers, that corresponds to lower density for maximal current. Further, the particle-hole symmetry in the system forces the density for maximal current to be greater than 0.5.

It has been noticed that the the bulk current-density curve remains qualitatively the same under different values of θ (except $\theta = 0$) (see figure 3(a)). For consideration of the maximum effect of energy E on both the rates q and r , we choose $\theta = 0.5$ in the future calculations. Moreover, for $\theta = 0.5$, the critical energy is given as $E_c = -2.885k_B T$, as was also found before in [31].

The bulk current-density relation obtained in equation (13) has been further analyzed with a 3D plot in figure 3(b) for various values of interaction energy E . The cluster mean-field results are found to be in agreement with the Monte Carlo simulations. The results signify that in the case of attractive and weak repulsive interactions, the particle current is a unimodal function of ρ with maximum occurring at $\rho = 0.5$ while for the case of stronger repulsions, it changes its nature to the bimodal function of ρ , indicated by the double-hump like structures in the curves. Moreover, here $\rho = 0.5$ becomes the point of local minimum. Thus, it can be concluded that for the proposed system interactions can significantly affect the bulk dynamical properties such as current-density relation. Further, the density diagram of particle current as a function of interaction energy E and density ρ computed analytically from equation (13) is displayed in figure 4. It is found that the particle current is maximum at $\rho = 0.5$ and $E \approx -1.3k_B T$ represented at the point A in figure 4. Moreover, it can also be seen that $\rho = 0.5$ is the line of maximal current for $E > E_c$, while for values of E lesser than E_c , it becomes the line of minimal current. It is worthwhile to note that in comparison to the theoretical results for the interaction energy corresponding to the maximal current in [36, 37], the predicted result $E \approx -1.3k_B T$ by two-cmf is in very good agreement with simulations indicating $E \approx -1.25k_B T$. This implies that the two-cmf theory is stronger and handles correlations better than the theories discussed in [36, 37].

The analysis of our results in figures 2–4 imply that the two-cmf results match exactly with simulations for moderate repulsions and weak attractions. However, for the case of stronger interactions, the results of two-cmf are in qualitative agreement with simulations. This suggests the consideration of three-cluster mean-field analysis, which treats the correlations between three-consecutive lattice sites exactly.

3.2. Three cluster mean-field theory

In this section, we study the bulk current-density relation using three cluster mean-field (three-cmf) approximation that assumes

$$P(\tau_{i-2}, \tau_{i-1}, \tau_i, \tau_{i+1}, \tau_{i+2}, \tau_{i+3}) = P(\tau_{i-2} | \tau_{i-1}, \tau_i) P(\tau_{i-1} | \tau_i, \tau_{i+1}) P(\tau_i, \tau_{i+1}, \tau_{i+2}) \times P(\tau_{i+1}, \tau_{i+2} | \tau_{i+3}), \tag{19}$$

where

$$P(\tau_{i-2} | \tau_{i-1}, \tau_i) = \frac{P(\tau_{i-2}, \tau_{i-1}, \tau_i)}{\sum_{\tau_{i-2} \in \{0,1\}} P(\tau_{i-2}, \tau_{i-1}, \tau_i)}. \tag{20}$$

The possible three-cluster probabilities $P(1, 1, 1)$, $P(1, 1, 0)$, $P(1, 0, 1)$, $P(1, 0, 0)$, $P(0, 1, 1)$, $P(0, 1, 0)$, $P(0, 0, 1)$, and $P(0, 0, 0)$ can respectively, be denoted by a , b , c , d , e , f , g and h . The normality condition for these probabilities implies

$$a + b + c + d + e + f + g + h = 1. \tag{21}$$

Using the general Kolmogorov consistency conditions [39]

$$\sum_{\tau=0}^1 P(\tau_1, \tau_2, \dots, \tau_{n-1}, \tau) = P(\tau_1, \tau_2, \dots, \tau_{n-1}) = \sum_{\tau=0}^1 P(\tau, \tau_1, \tau_2, \dots, \tau_{n-1}), \tag{22}$$

for $n = 3$, we obtain the following four equations

$$\begin{aligned} P(1, 1, 0) + P(1, 1, 1) &= P(0, 1, 1) + P(1, 1, 1), \\ P(1, 0, 0) + P(1, 0, 1) &= P(0, 1, 0) + P(1, 1, 0), \\ P(0, 1, 0) + P(0, 1, 1) &= P(0, 0, 1) + P(1, 0, 1), \\ P(0, 0, 0) + P(0, 0, 1) &= P(0, 0, 0) + P(1, 0, 0), \end{aligned} \tag{23}$$

which are further simplified to

$$b = e, \tag{24}$$

$$d = g, \tag{25}$$

$$d + c = f + b. \tag{26}$$

Moreover, the consistency condition along with the definition of density imply

$$\rho = a + b + c + d. \tag{27}$$

Utilizing equations (19), (21), (24)–(27) in equation (1), the bulk particle current, under three-cmf, reduces to

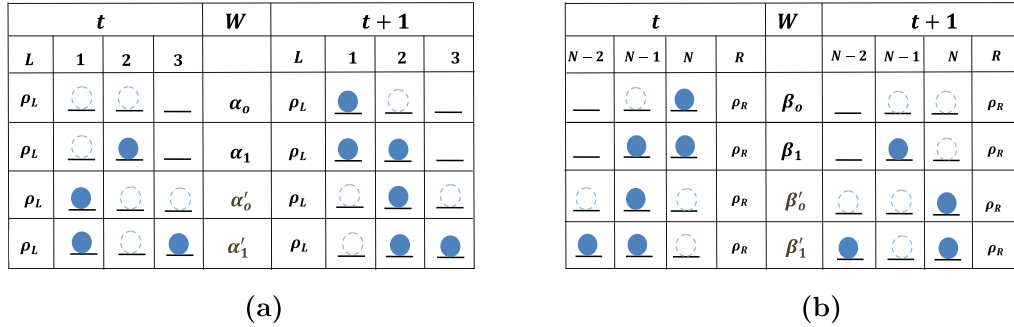


Figure 5. Sketch of evolution of (a) the first site (b) the N th of the lattice, from time step t to $(t + 1)$ under different possible configurations with corresponding transition probabilities denoted by W . No circle at a site means the site can either be empty or occupied. Here, ρ_L and ρ_R , respectively, denote the densities of left (L) and right (R) boundary reservoir.

$$J = \frac{f(d + qc) + b(rd + c)}{(d + c)}. \tag{28}$$

Using equation (3), we obtain the master equation for $b = P(1, 1, 0)$, $a = P(1, 1, 1)$ and $h = P(0, 0, 0)$, each of which in the steady-state reduces, respectively, to

$$\begin{aligned} &P(1, 1, 0, 1, 0) + P(1, 1, 1, 0, 1) + qP(0, 1, 0, 1, 0) + rP(1, 1, 1, 0, 0) \\ &- P(1, 1, 0, 1) - rP(1, 1, 0, 0) = 0, \\ &P(1, 1, 0, 1, 1) + qP(0, 1, 0, 1, 1) - rP(1, 1, 1, 0, 0) - P(1, 1, 1, 0, 1) = 0 \text{ and} \\ &P(0, 0, 1, 0, 0) + qP(0, 0, 1, 0, 1) - P(0, 1, 0, 0, 0) - rP(1, 1, 0, 0, 0) = 0. \end{aligned}$$

Using the three-cmf analysis (equations (19) and (20)), the above three equations, respectively, reduces to

$$\begin{aligned} &cf(a + e)(qc + b) - eb(rd + c)(d + c) = 0, \\ &ce(a + e)(qf + b) - ab(e + f)(rd + c) = 0, \\ &fg(d + h)(d + qc) - dh(e + f)(rb + f) = 0. \end{aligned} \tag{29}$$

To obtain the particle-current in equation (28) as a function of density ρ , we need to solve equations (24)–(29) and determine the unknowns a, b, \dots, h in terms of density ρ . But the complexity and the non-linearity involved in these equations forbid their analytical solution. However, the particle current and the unknown probabilities can be numerically computed for any value of interaction energy E and density ρ . Interestingly, for the case of weak attractions and moderate repulsions, the numerically computed current from the three-cmf theory matches exactly with the current obtained analytically from the two-cmf theory, indicating the two-cmf to be exact in this case. Whereas for stronger interactions, the theory is approximate due to the qualitative agreement of results with the simulations. In the upcoming sections, we analyze and discuss the effect of interactions and correlations on the open system utilizing the simpler two-cmf approach.

4. Particles locomotion in open system

In the previous section, we analyzed the role of interactions on the steady-state bulk-properties by considering the closed system. In this section, we couple the lattice ends with reservoirs of fixed density to study the effect of open boundaries. The boundary acts as an inhomogeneity to the system in a way that the interaction of the particles with boundary reservoirs leads to different dynamics. In the open system, we have considered the rates for the jumps from sites $i = 2, 3, \dots, N - 2$ similar to that of the closed system, discussed in section 2.1. Coupling to the reservoirs are taken into account such that the injection from the left reservoir of density ρ_L and ejection to the right reservoir with density ρ_R occur, respectively, for sites 1 and N . The entry and exit rules for sites 1 and N are defined as follows. A particle enters to site 1 with the rate α_0 (α_1) if the site 2 is empty (occupied). Whereas, it hops from the first site with the rates $\alpha'_{0,1}$ depending on the occupancy state of site 3 as vacant/occupied (see figure 5(a)). Similarly, the exit rate from site N is $\beta_{0,1}$ when the site $N - 1$ is empty/occupied and the rate of entering to site N from site $N - 1$ is $\beta'_{0,1}$ when site $N - 2$ is empty/occupied (see figure 5(b)). Thus, the steady-state bulk current $J_{i,i+1}$ from site i to $(i + 1)$, $i = 2, 3, \dots, N - 2$ is given by

$$J_{i,i+1} = P(0, 1, 0, 0) + qP(0, 1, 0, 1) + rP(1, 1, 0, 0) + P(1, 1, 0, 1),$$

which is same as equation (1). Similarly, the flux (current) in and out for both the sites 1 and N can be written as

$$J_{L,1} = \alpha_0 P(0, 0) + \alpha_1 P(0, 1), \quad (30)$$

$$J_{1,2} = \alpha'_0 P(1, 0, 0) + \alpha'_1 P(1, 0, 1), \quad (31)$$

$$J_{N-1,N} = \beta'_0 P(0, 1, 0) + \beta'_1 P(1, 1, 0), \quad (32)$$

$$J_{N,R} = \beta_0 P(0, 1) + \beta_1 P(1, 1), \quad (33)$$

where $J_{i,j}$ represent the flow of particles from i th to j th site. Here, L and R , respectively denote the left and right reservoir. Using the two-cmf analysis (equations (4) and (5)), the above equations reduce to

$$J_{L,1} = \alpha_0 z + \alpha_1 y, \quad (34)$$

$$J_{1,2} = \frac{y(\alpha'_0 z + \alpha'_1 y)}{(1 - \rho)}, \quad (35)$$

$$J_{N-1,N} = \frac{y(\beta'_0 y + \beta'_1 x)}{\rho}, \quad (36)$$

$$J_{N,R} = \beta_0 y + \beta_1 x. \quad (37)$$

5. Bulk-adapted coupling and NESS phases

The kind of coupling conditions to the reservoirs for open systems has a strong effect on the steady-state phase diagrams. We recall that the thermodynamically consistent open boundary conditions utilized in [36, 37], whose bulk-dynamical rules are same as that of our model, produce the phase diagrams with only three stationary phases, namely, low-density (*LD*), high-density (*HD*) and maximal current (*MC*), irrespective of the strength of interaction energy. While the application of minimum and maximum current principles to the bulk current-density relation suggests the dependency of the number of phases on the interaction strength [11, 13, 28]. In this section, we embrace the bulk-adapted coupling to the reservoirs, which considers the relation between the density and the correlators near the system boundaries to be same as in the bulk [32] and analyze the open system using the two-cmf approach. These boundary conditions are not thermodynamically consistent, but the benefit of such coupling of the system to the reservoirs is that the steady-state phase diagrams constructed from the extremal current principles become valid. In such coupling environment, the number of stationary phases depends strongly on the nature and the strength of interactions.

In the bulk adapted coupling, the lattice is viewed as being continued into the left (*L*) and right (*R*) reservoirs, corresponding to the relation between the correlators $\langle \tau_{i-1} \tau_i \tau_{i+1} \tau_{i+2} \rangle$ and density $\rho = \langle \tau_i \rangle$ in the bulk [32]. Since the bulk hoppings in the system consider the four point correlators, so to define the entry and exit rates for both the sites 1 and *N* in accordance with the bulk rates, the missing nearest or next-nearest-neighboring sites of 1 and *N* need to be fictitiously created. The rates α_k , α'_k and β_k , β'_k ($k = \{0, 1\}$) depend on the reservoir densities ρ_L and ρ_R , respectively and for site 1, in particular, they can be understood as follows. As discussed in section 2 that if the configuration $(\tau_{i+1} = 0, \tau_{i+2})$ exists in the bulk, a particle at *i*th site can hop with rate $q^{\tau_{i+2}}$ when $\tau_{i-1} = 0$, otherwise the hopping rate is $r^{(1-\tau_{i+2})}$. For a given configuration $(\tau_{i+1} = 0, \tau_{i+2})$ with probability $P(\tau_{i+1} = 0, \tau_{i+2}) > 0$, we define the conditional probabilities for configuration $(\tau_{i-1}, \tau_i = 1)$ to occur in the NESS of a closed system with density ρ as $P(0, 1 | 0, \tau_{i+2}; \rho) = \frac{P(0, 1, 0, \tau_{i+2}; \rho)}{P(0, \tau_{i+2}; \rho)}$ when $\tau_{i-1} = 0$ and $P(1, 1 | 0, \tau_{i+2}; \rho) = \frac{P(1, 1, 0, \tau_{i+2}; \rho)}{P(0, \tau_{i+2}; \rho)}$ when $\tau_{i-1} = 1$. The injection rate, α_{τ_2} , to site 1, is obtained from a weighting of rates with the probabilities $P(0, 1 | 0, \tau_2; \rho_L)$ and $P(1, 1 | 0, \tau_2; \rho_L)$ corresponding to virtual configurations $\{\tau_{-1} = 0, \tau_0 = 1, \tau_1 = 0, \tau_2\}$ and $\{\tau_{-1} = 1, \tau_0 = 1, \tau_1 = 0, \tau_2\}$, respectively at the boundaries. Similarly, the hopping rate, α'_{τ_3} , from site 1 to site 2 results from a weighting of rates with probability $P(0|1, 0, \tau_3; \rho_L)$ and $P(1|1, 0, \tau_3; \rho_L)$ for virtual configurations $\{\tau_0 = 0, \tau_1 = 1, \tau_2 = 0, \tau_3\}$ and $\{\tau_0 = 1, \tau_1 = 1, \tau_2 = 0, \tau_3\}$, respectively. Thus, for $k = \{0, 1\}$,

$$\begin{aligned} \alpha_k &= q^k P(0, 1 | 0, k; \rho_L) + r^{(1-k)} P(1, 1 | 0, k; \rho_L), \\ \alpha'_k &= q^k P(0 | 1, 0, k; \rho_L) + r^{(1-k)} P(1 | 1, 0, k; \rho_L). \end{aligned} \quad (38)$$

Similarly, the rates for in and out from site *N*, β_k and β'_k , where $k = \{0, 1\}$, are defined as

$$\beta_k = r^k \bar{P}(0, 0 | 1, k; \rho_R) + q^{(1-k)} \bar{P}(1, 0 | 1, k; \rho_R), \quad (39)$$

$$\beta'_k = r^k \bar{P}(0 | 0, 1, k; \rho_R) + q^{(1-k)} \bar{P}(1 | 0, 1, k; \rho_R). \quad (40)$$

The conditional probability, involved in the entrance and exit rates for site N , such as $\bar{P}(0, 0 | 1, k; \rho_R)$ is inferred as $\frac{P(k, 1, 0; \rho_R)}{P(k, 1; \rho_R)}$ for the virtual configuration $\{\tau_{N-1} = k, \tau_N = 1, \tau_{N+1} = 0, \tau_{N+2} = 0\}$ and given configuration $\{\tau_{N-1} = k, \tau_N = 1\}$. Similarly, the other involved probabilities can be understood. Using two-cmf analysis from equation (5) and equation (4), the input and output rates are written as

$$\alpha_k = \frac{y_L(q^k y_L + r^{(1-k)} x_L)}{\rho_L(1 - \rho_L)}, \quad (41)$$

$$\alpha'_k = \frac{q^k y_L + r^{(1-k)} x_L}{\rho_L}, \quad (42)$$

$$\beta_k = \frac{y_R(r^k z_R + q^{(1-k)} y_R)}{\rho_R(1 - \rho_R)}, \quad (43)$$

$$\beta'_k = \frac{r^k z_R + q^{(1-k)} y_R}{1 - \rho_R}, \quad (44)$$

where $k = \{0, 1\}$ and $x_{L/R}$, $y_{L/R}$ and $z_{L/R}$ are computed from equations (10)–(12) for $\rho = \rho_{L/R}$.

The above defined bulk-adapted coupling to the reservoirs allows one to obtain the steady-state phase diagram by applying the minimum and maximum current principles [11, 13, 28]. In figure 6(a), we plot the bulk current-density relation in NESS, computed using two-cmf in section 3.1 for interaction energy $E = -5k_B T < E_c$. Clearly, the fundamental diagram exhibits three extrema: two of them corresponding to the maximal current, marked by ρ_1^* and ρ_2^* , and one corresponds to the point of local minimum in the density range (ρ'_1, ρ'_2) . Further, figure 6 (b) shows that the boundary-induced phase diagram with seven stationary phases as predicted from extremal current principles is in good agreement with the simulation results. However, small deviations occur due to the approximate bulk current-density relation produced by two-cmf analysis. Thus, it can be concluded that for $E \leq E_c = -2.885k_B T$, the boundary induced phase diagram has seven phases, namely, two maximal current phases (MC_1 and MC_2) with respective bulk densities as ρ_1^* and ρ_2^* , one minimal current phase (MC_3) with bulk density as $\rho = 0.5$, two LD and two HD phases, with bulk densities as ρ_L and ρ_R , respectively. The transition between any of the two phases is either first-order or second-order continuous as indicated by solid and dotted lines, respectively, in figure 6(b). Since for $E > E_c$, the particle current density curve has only one extremum i.e. $\rho = 0.5$, which corresponds to the maximal current, the corresponding steady-state phase diagram of open system has only three phases: (MC) phase with bulk density $\rho = 0.5$ for $\rho_L > 0.5$, LD phase for $\rho = \rho_L < 0.5$ and HD phase for $\rho = 1 - \rho_R > 0.5$. This shows the importance of the nature of interactions and type of coupling conditions on system's dynamical properties.

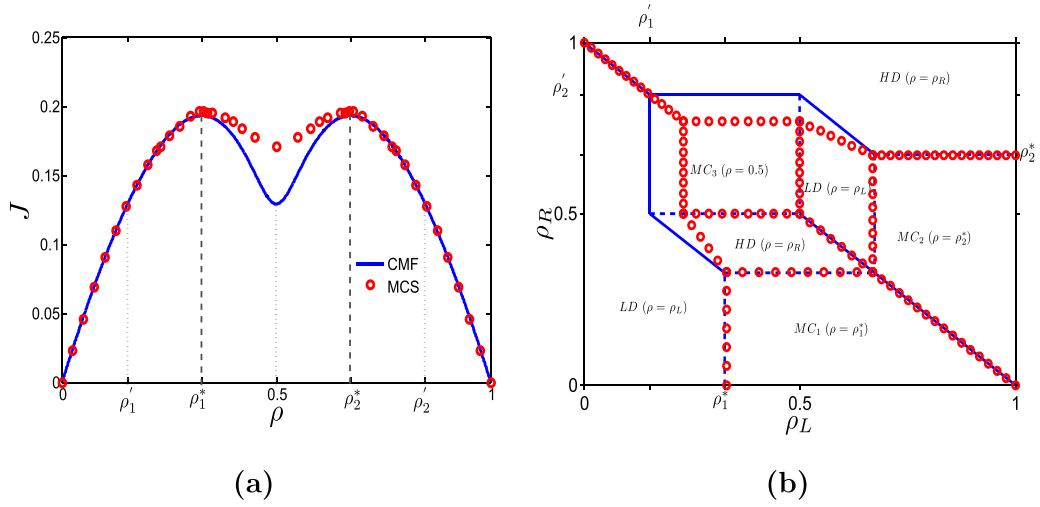


Figure 6. (a) Fundamental diagram of particle current (J_{\max}) versus density ρ , (b) Phase diagram of the open interactive TASEP system, for $E = -5k_B T$ and $\theta = 0.5$. Solid and dotted lines, respectively represent the first and second order phase transition lines.

6. Correlations

In this section, we compute the two-point classical correlation function between sites i and j , where $(1 \leq i \neq j \leq N)$, defined by

$$C = \langle \tau_i \tau_j \rangle - \langle \tau_i \rangle \langle \tau_j \rangle, \tag{45}$$

where the two-point and the one-point density functions are given as

$$\langle \tau_i \tau_j \rangle = \sum_{\tau_i} \sum_{\tau_j} \tau_i \tau_j P(\tau_i, \tau_j) = P(\tau_i = 1, \tau_j = 1) \tag{46}$$

and

$$\langle \tau_i \rangle = \sum_{\tau_i} \tau_i P(\tau_i) = \rho. \tag{47}$$

Physically, the correlation function C , measures the effect of the particle at i th site on the occupancy state of j th site. If the distance between sites i and j is n i.e. sites i and j are separated by n sites, then the function C can be written as

$$C(n) = \sum_{\tau_1, \tau_2, \dots, \tau_{n-1}} P(\tau_i = 1, \tau_1, \tau_2, \dots, \tau_{n-1}, \tau_j = 1) - \rho^2, \tag{48}$$

where $\tau_1, \tau_2, \dots, \tau_{n-1} \in \{0, 1\}$. For simplification, we denote $\sum_{\tau_1, \tau_2, \dots, \tau_{n-1}} P(\tau_i = 1, \tau_1, \tau_2, \dots, \tau_{n-1}, \tau_j = 1)$ by t_n . Then, using the two-cmf analysis, we obtain $t_1 = x$, $t_2 = \frac{y^2}{1-\rho} + \frac{x^2}{\rho}$ and t_n for $n > 2$ (see appendix) reduces to

$$t_n = \left(\frac{x}{\rho} + \frac{z}{1-\rho} \right) t_{n-1} + \frac{x}{\rho} \left(\frac{y^2}{x(1-\rho)} - \frac{z}{1-\rho} \right) t_{n-2}. \tag{49}$$

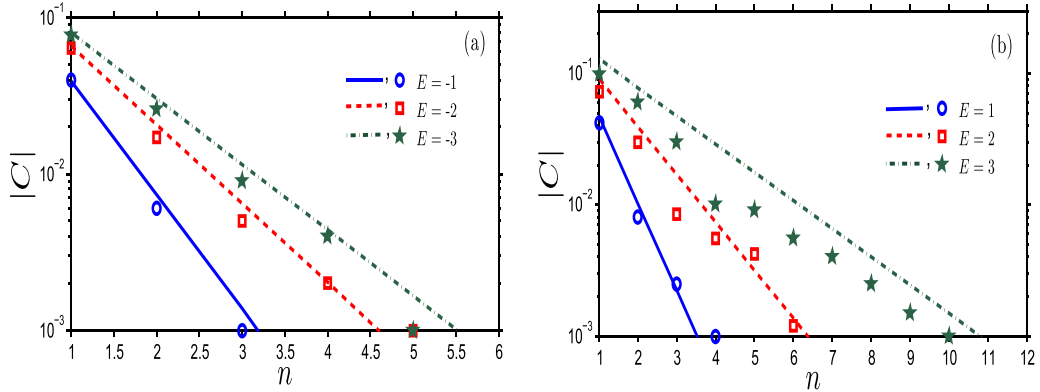


Figure 7. Plot of absolute value of correlation function (C) versus distance n for (a) repulsive (b) attractive energy measured in $k_B T$. Lines are the interpolation of analytical results at different n , while symbols represent the simulation results.

Substituting equation (49) into equation (48) and using the notation $u = \frac{x}{\rho} + \frac{z}{1-\rho}$ and relation

$$\left(\frac{x}{\rho} + \frac{z}{1-\rho}\right) + \frac{x}{\rho} \left(\frac{y^2}{x(1-\rho)} - \frac{z}{1-\rho}\right) = 1, \quad (50)$$

the correlation function given by equation (48) produces the following second-order linear homogeneous recurrence relation

$$C(n) = uC(n-1) + (1-u)C(n-2), \quad \text{for } n > 2. \quad (51)$$

Solving the above relation for conditions $C(1) = x - \rho^2$ and $C(2) = \frac{y^2}{1-\rho} + \frac{x^2}{\rho} - \rho^2$ yields $C(n) = \rho(1-\rho) \left(1 + \frac{y}{\rho(\rho-1)}\right)^n$. Clearly, $C(n) \rightarrow 0$ for $E \rightarrow 0$ (or $y \rightarrow \rho(1-\rho)$).

Moreover, using the equation (10), the classical two point nearest neighbor correlation between two consecutive sites, denoted by $C(1)$, can be written as

$$C(1) = \begin{cases} \frac{r+2\rho(1-\rho)(q-r) - \sqrt{r(r(1-2\rho)^2 + 4q\rho(1-\rho))}}{2(q-r)}, & q, r \neq 1 \\ 0, & q, r = 1. \end{cases} \quad (52)$$

The semi-dotted curve and symbols initiating from the right hand side of figure 2(b) shows the two-point nearest neighbor correlation ($C(1)$), computed from two-cmf and simulations, respectively, in the maximal current phase as a function of interaction energy $E, k_B T$. It is interesting to note that the nearest neighbor correlations first decreases with the decrease in interaction energy from $7k_B T$ as shown in figure 2(b), becomes minimum for $E_c = -2.885k_B T$ and then starts increasing for higher values of repulsive interaction energy. Further, it is fascinating to see that the maximal particle flux occurring at $E = -1.3k_B T$ does not corresponds to the interaction energy for minimum correlations. To explain this observation, we note that the minimum of correlations observed in figure 2(b) corresponds to the maximum in the anti-correlation. This means that at this interaction strength ($-2.885 k_B T$) the system prefers to have the alternating particles and holes, i.e. 101010 configurations. But then the flux depends

mostly on the rate q , which is quite small at these conditions. Lowering the repulsion increases the rate q , but simultaneously, as one can see from figure 2(b), it decreases the fraction of alternating configurations. The interplay between these two trends determines the position of the maximal particle current.

Moreover, the curves in figures 2(b), 3(b) and 6 indicate that the simulation results are in agreement with the cluster mean-field results for repulsions and weak attractions while for stronger interactions, the results match qualitatively. The reason for such behavior can be analyzed by calculating $C(n)$ for repulsive and attractive interactions (see figure 7). It can be seen that effect of a particle's presence on one site to other site decreases exponentially as the distance between the sites increases [40]. However, for the repulsive interactions, the correlation dies out faster (i.e. for a comparatively smaller n) than the attractive interactions. This indicates that the correlations are *short-range* for repulsions, while they are *long-range* in the case of attractions. This is also physically justified since for the case of attractions, the particles group together to form a large cluster, which implies that the presence of particle at first site of the cluster affects the occupancy of far apart sites. However, for repulsions, the particles tend to isolate, that causes the correlation to be short-range and weak for the distant sites. As the two-cmf theory considers the short-range i.e. two nearest neighboring sites correlations, the theory fits well for the repulsions and weak attractions. For the case of higher attractions, one requires a more advanced theory.

7. Conclusion

To summarize, we have considered a 1D TASEP model incorporating the effect of repulsive as well as attractive nearest neighbor inter-particle interactions in accordance with the thermodynamic consistent rules. The bulk hopping rules of our model are more general and are different from [31–33], that require the sum of the bond breaking rate and the bond making rate to be equal to the sum of the rates corresponding to the situations: when neither bond-breaking nor bond-making occur and when both of them happen simultaneously. The system is analyzed theoretically using the two-cluster mean-field approximation for both periodic and open boundary conditions. The approach treats the nearest neighbor correlation exactly and is different from the approaches presented in [31–33, 36, 37]. The influence of interactions on bulk current-density relation has been thoroughly scrutinized. Interestingly, the bulk current-density relation is perceived as a unimodal function for the case of attractions and weak repulsions and it changed its nature to a bimodal function (with equal modes) after a critical value of repulsive interaction energy, which was not found in [36, 37] whose bulk dynamical rules are the same as that of our model. The reason for two equal modes at densities less than and greater than 0.5 is the particle-hole symmetry prevailing in the system and the reduction of the model to TASEP with dimers for the case of stronger repulsions that reduces the maximal particle density to less than 0.5. The role of interactions is also observed on the maximal particle current that dies for the case of large attractive interactions and saturates for stronger repulsions. Moreover, the particle current computed from two-cmf is found to be maximum for a weak

repulsive interaction strength $E \approx -1.3k_B T$, which matches with the simulations. It implies that the proposed two-cmf approach describes the system better than the theories in [36] and [37] which predicted the optimal interaction strength as $E \approx -3k_B T$ and $E \approx -0.9k_B T$, respectively. All the system's properties are also investigated using three-cluster mean-field theory, whose numerical calculations match precisely with the analytical results obtained from the two-cmf for the case of moderate repulsions and weak attractive interactions. Further, in this case, the results also matched exactly with Monte Carlo simulations implying the predictions from the two-cmf theory to be exact. However, for stronger interactions, there is only a qualitative agreement between simulations and the two theories.

The steady-state phase diagram for interactive systems has not been easy to retrieve. The application of maximum and minimum current principles to the bulk current-density relation predicts seven phases in the phase diagram for stronger repulsions, while the simulation results for an open boundary condition as in [36, 37] yields only three stationary phases. For validating the phase diagram predicted from extremal current principles and for testing the effect of thermodynamic constraints in the boundary conditions, we have deliberately chosen the bulk-adapted coupling to the reservoirs [32]. The simulations, as well as theoretical results, then indicate three phases in the phase diagram for the case of attraction and weak repulsion, while seven generic phases are predicted for the stronger repulsive interactions. However, the approximate nature of bulk current-density relation brings out small discrepancies between the two-cmf and the simulation results for the case of stronger interactions. We have also computed the correlations between two lattice sites as a function of the distance between them and found the correlations to decrease exponentially for both attractive and repulsive interactions. Moreover, they are observed to be *short-range* for repulsion and *long-range* for the case of attractions.

Acknowledgment

We are thankful to both the anonymous referees for their valuable suggestions in improving the quality of the manuscript. ABK acknowledges the support from the Welch Foundation (Grant C-1559), from the NSF (Grant CHE-1664218), and the Center for Theoretical Biological Physics sponsored by the NSF (Grant PHY-1427654).

Appendix. Calculation of t_n

$$t_n = \sum_{\tau_1, \tau_2, \dots, \tau_{n-2}} P(1, \tau_1, \tau_2, \dots, \tau_{n-2}, 1, 1) + \sum_{\tau_1, \tau_2, \dots, \tau_{n-2}} P(1, \tau_1, \tau_2, \dots, \tau_{n-2}, 0, 1). \quad (\text{A.1})$$

Using equations (4) and (5), we get

$$\begin{aligned} P(1, \tau_1, \tau_2, \dots, \tau_{n-2}, 1, 1) &= P(1, \tau_1) P(\underline{\tau}_1 | \tau_2) \cdots P(\tau_{n-3} | \tau_{n-2}) P(\tau_{n-2} | 1) P(\underline{1} | 1) \\ &= P(1, \tau_1, \tau_2, \dots, \tau_{n-3}, \tau_{n-2}, 1) P(\underline{1} | 1) \end{aligned} \quad (\text{A.2})$$

and

$$\begin{aligned}
 P(1, \tau_1, \tau_2, \dots, \tau_{n-2}, 0, 1) &= P(1, \tau_1)P(\tau_1 | \tau_2) \cdots P(\tau_{n-3} | \tau_{n-2})P(\tau_{n-2} | 0)P(0 | \tau_1) \\
 &= P(1, \tau_1, \tau_2, \dots, \tau_{n-3}, \tau_{n-2}, 1) \frac{P(\tau_{n-2} | 0)P(0 | 1)}{P(\tau_{n-2} | 1)}, \tag{A.3}
 \end{aligned}$$

which implies

$$\begin{aligned}
 t_n &= \sum_{\tau_1, \tau_2, \dots, \tau_{n-2}} P(1, \tau_1, \tau_2, \dots, \tau_{n-2}, 1) \left(\frac{x}{\rho} + \frac{yP(\tau_{n-2}, 0)}{(1-\rho)P(\tau_{n-2}, 1)} \right) \\
 &= \sum_{\tau_1, \tau_2, \dots, \tau_{n-3}} P(1, \tau_1, \tau_2, \dots, \tau_{n-3}, 1, 1) \left(\frac{x}{\rho} + \frac{yP(1, 0)}{P(1, 1)(1-\rho)} \right) \\
 &\quad + \sum_{\tau_1, \tau_2, \dots, \tau_{n-3}} P(1, \tau_1, \tau_2, \dots, \tau_{n-3}, 0, 1) \left(\frac{x}{\rho} + \frac{P(0, 0)}{(1-\rho)} \right) \\
 &= \left(\frac{x}{\rho} + \frac{y^2}{x(1-\rho)} \right) \sum_{\tau_1, \tau_2, \dots, \tau_{n-3}} P(1, \tau_1, \tau_2, \dots, \tau_{n-3}, 1, 1) + \left(\frac{x}{\rho} + \frac{z}{(1-\rho)} \right) \\
 &\quad \times \left(\sum_{\tau_1, \tau_2, \dots, \tau_{n-2}} P(1, \tau_1, \tau_2, \dots, \tau_{n-2}, 1) - \sum_{\tau_1, \tau_2, \dots, \tau_{n-3}} P(1, \tau_1, \tau_2, \dots, \tau_{n-3}, 1, 1) \right) \\
 &= \left(\frac{x}{\rho} + \frac{z}{(1-\rho)} \right) \sum_{\tau_1, \tau_2, \dots, \tau_{n-2}} P(1, \tau_1, \tau_2, \dots, \tau_{n-2}, 1) \\
 &\quad + \left(\frac{y^2}{x(1-\rho)} - \frac{z}{(1-\rho)} \right) \sum_{\tau_1, \tau_2, \dots, \tau_{n-3}} P(1, \tau_1, \tau_2, \dots, \tau_{n-3}, 1, 1). \tag{A.4}
 \end{aligned}$$

Using equation (A.2), we get

$$\begin{aligned}
 t_n &= \left(\frac{x}{\rho} + \frac{z}{(1-\rho)} \right) \sum_{\tau_1, \tau_2, \dots, \tau_{n-2}} P(1, \tau_1, \tau_2, \dots, \tau_{n-2}, 1) \\
 &\quad + \frac{x}{\rho} \left(\frac{y^2}{x(1-\rho)} - \frac{z}{(1-\rho)} \right) \sum_{\tau_1, \tau_2, \dots, \tau_{n-3}} P(1, \tau_1, \tau_2, \dots, \tau_{n-3}, 1), \tag{A.5}
 \end{aligned}$$

which further gives

$$t_n = \left(\frac{x}{\rho} + \frac{z}{(1-\rho)} \right) t_{n-1} + \frac{x}{\rho} \left(\frac{y^2}{x(1-\rho)} - \frac{z}{(1-\rho)} \right) t_{n-2}. \tag{A.6}$$

References

- [1] Lipowsky R *et al* 2001 *Phys. Rev. Lett.* **87** 108101
- [2] Zia R K P *et al* 2011 arXiv:1108.3312
- [3] Chou T and Lakatos G 2004 *Phys. Rev. Lett.* **93** 198101
- [4] Chou T and Lohse D 1999 *Phys. Rev. Lett.* **82** 3552
- [5] Klumpp S and Lipowsky R 2003 *J. Stat. Phys.* **113** 233–68
- [6] Hilhorst H J and Appert-Rolland C 2012 *J. Stat. Mech.* P06009
- [7] Katz S, Lebowitz J L and Spohn H 1983 *Phys. Rev. B* **28** 1655
- [8] Chowdhury D, Schadschneider A and Nishinari K 2005 *Phys. Life Rev.* **2** 318–52

- [9] MacDonald C T, Gibbs J H and Pipkin A C 1968 *Biopolymers* **6** 1–25
- [10] Derrida B 1998 *Phys. Rep.* **301** 65–83
- [11] Krug J 1991 *Phys. Rev. Lett.* **67** 1882
- [12] Schütz G and Domany E 1993 *J. Stat. Phys.* **72** 277–96
- [13] Popkov V and Schütz G M 1999 *Europhys. Lett.* **48** 257
- [14] Evans M R, Juhász R and Santen L 2003 *Phys. Rev. E* **68** 026117
- [15] Derrida B, Evans M R, Hakim V and Pasquier V 1993 *J. Phys. A: Math. Gen.* **26** 1493
- [16] Kolomeisky A B, Schütz G M, Kolomeisky E B and Straley J P 1998 *J. Phys. A: Math. Gen.* **31** 6911
- [17] Derrida B, Domany E and Mukamel D 1992 *J. Stat. Phys.* **69** 667–87
- [18] Blythe R A and Evans M R 2007 *J. Phys. A: Math. Theor.* **40** R333
- [19] Schmittmann B and Zia R K P 1995 *Phase Transit. Crit. Phenom.* **17** 3–214
- [20] Helbing D 2001 *Rev. Mod. Phys.* **73** 1067
- [21] Appert-Rolland C, Ebbinghaus M and Santen L 2015 *Phys. Rep.* **593** 1–59
- [22] Chowdhury D 2013 *Phys. Rep.* **529** 1–197
- [23] Kolomeisky A B 2013 *J. Phys.: Condens. Matter* **25** 463101
- [24] Kolomeisky A B 2015 *Motor Proteins and Molecular Motors* (Boca Raton, FL: CRC Press)
- [25] Roos W H *et al* 2008 *Phys. Biol.* **5** 046004
- [26] Vilfan A, Frey E, Schwabl F, Thormählen M, Song Y H and Mandelkow E 2001 *J. Mol. Biol.* **312** 1011–26
- [27] Seitz A and Surrey T 2006 *EMBO J.* **25** 267–77
- [28] Hager J, Krug J, Popkov V and Schütz G 2001 *Phys. Rev. E* **63** 056110
- [29] Antal T and Schütz G 2000 *Phys. Rev. E* **62** 83
- [30] Klumpp S and Lipowsky R 2004 *Europhys. Lett.* **66** 90
- [31] Dierl M, Maass P and Einax M 2011 *Europhys. Lett.* **93** 50003
- [32] Dierl M, Maass P and Einax M 2012 *Phys. Rev. Lett.* **108** 060603
- [33] Dierl M, Einax M and Maass P 2013 *Phys. Rev. E* **87** 062126
- [34] Katz S, Lebowitz J L and Spohn H 1984 *J. Stat. Phys.* **34** 497–537
- [35] Pinkoviezky I and Gov N S 2013 *New J. Phys.* **15** 025009
- [36] Teimouri H, Kolomeisky A B and Mehrabiani K 2015 *J. Phys. A: Math. Theor.* **48** 065001
- [37] Celis-Garza D, Teimouri H and Kolomeisky A B 2015 *J. Stat. Mech.* P04013
- [38] Chowdhury D, Santen L and Schadschneider A 2000 *Phys. Rep.* **329** 199–329
- [39] Gutowitz H A, Victor J D and Knight B W 1987 *Physica D* **28** 18–48
- [40] Hao Q Y, Jiang R, Hu M B, Jia B and Wang W X 2016 *Sci. Rep.* **6** 19652
- [41] Lakatos G and Chou T 2003 *J. Phys. A: Math. Gen.* **36** 2027